Monthly Notices of the ROYAL ASTRONOMICAL SOCIETY
MNRAS **445,** 3848–3861 (2014) doi:10.1093/mnras/stu1959

Detailed modelling of a large sample of *Herschel* sources in the Lockman Hole: identification of cold dust and of lensing candidates through their anomalous SEDs⋆

Michael Rowan-Robinson,[1†] Lingyu Wang,[2] Julie Wardlow,[3] Duncan Farrah,[4] Seb Oliver,[5] Jamie Bock,[6,7] Charlotte Clarke,[5] David Clements,[1] Edo Ibar,[8] Eduardo Gonzalez-Solares,[9] Lucia Marchetti,[10] Douglas Scott,[11] Anthony Smith,[5] Mattia Vaccari[12] and Ivan Valtchanov[13]

[1]*Astrophysics Group, Imperial College London, Blackett Laboratory, Prince Consort Road, London SW7 2AZ, UK*
[2]*Department of Physics, Durham University, South Rd, Durham DH1 3LE, UK*
[3]*Dark Cosmology Centre, Niels Bohr Institute, University of Copenhagen, DK-2100, Copenhagen Ø, Denmark*
[4]*Department of Physics, Virginia Polytechnic Institute and State University, 850 West Campus Drive, Blacksburg, VA 24061, USA*
[5]*Astronomy Centre, Department of Physics & Astronomy, University of Sussex, Brighton BN1 9QH, UK*
[6]*California Institute of Technology, 1200 E. California Blvd, Pasadena, CA 91125, USA*
[7]*Jet Propulsion Laboratory, 4800 Oak Grove Drive, Pasadena, CA 91109, USA*
[8]*Instituto de Física y Astronomía, Universidad de Valparaíso, Avda. Gran Bretaña 1111, Valparaíso, Chile*
[9]*Institute of Astronomy, Madingley Road, Cambridge CB3 0HA, UK*
[10]*Department of Physical Sciences, Open University, Walton Hall, Milton Keynes MK7 6AA, UK*
[11]*Department of Physics & Astronomy, University of British Columbia, 6224 Agricultural Road, Vancouver, BC V6T 1Z1, Canada*
[12]*University of Western Cape, 7535 Belliville, Cape Town, South Africa*
[13]*Herschel Science Centre, European Space Astronomy Centre, Villanueva de la Cañada, E-28691 Madrid, Spain*

Accepted 2014 September 18. Received 2014 September 17; in original form 2014 May 6

ABSTRACT

We have studied in detail a sample of 967 SPIRE sources with 5σ detections at 350 and 500 μm and associations with *Spitzer*-SWIRE 24 μm galaxies in the HerMES-Lockman survey area, fitting their mid- and far-infrared, and submillimetre, spectral energy distributions (SEDs) in an automatic search with a set of six infrared templates. For almost 300 galaxies, we have modelled their SEDs individually to ensure the physicality of the fits. We confirm the need for the new cool and cold cirrus templates, and also of the young starburst template, introduced in earlier work. We also identify 109 lensing candidates via their anomalous SEDs and provide a set of colour–redshift constraints which allow lensing candidates to be identified from combined *Herschel* and *Spitzer* data. The picture that emerges of the submillimetre galaxy population is complex, comprising ultraluminous and hyperluminous starbursts, lower luminosity galaxies dominated by interstellar dust emission, lensed galaxies and galaxies with surprisingly cold (10–13 K) dust. 11 per cent of 500 μm selected sources are lensing candidates. 70 per cent of the unlensed sources are ultraluminous infrared galaxies and 26 per cent are hyperluminous. 34 per cent are dominated by optically thin interstellar dust ('cirrus') emission, but most of these are due to cooler dust than is characteristic of our Galaxy. At the highest infrared luminosities we see SEDs dominated by M82, Arp 220 and young starburst types, in roughly equal proportions.

Key words: gravitational lensing: strong – galaxies: evolution – galaxies: starburst – cosmology: observations – infrared: galaxies – submillimetre: galaxies.

1 INTRODUCTION

The combination of *Herschel* (Pilbratt et al. 2010) and *Spitzer* data provides us with the first 3–500 μm spectral energy distributions (SEDs) of large samples of galaxies, for which we can accurately determine the masses of cold dust and search for very young, heavily

⋆ *Herschel* is an ESA space observatory with science instruments provided by European-led Principal Investigator consortia and with important participation from NASA.

† E-mail: mrr@imperial.ac.uk

obscured starbursts. The HerMES (Herschel Multi-tiered Extragalactic Survey) wide-area surveys (Oliver et al. 2012) have been targeted on fields in which we already have excellent *Spitzer* data.

Over the past 20 years increasingly sophisticated radiative transfer models for different types of infrared galaxy have been developed, for example for starburst galaxies (Rowan-Robinson & Crawford 1989; Rowan-Robinson & Efstathiou 1993; Silva et al. 1998; Efstathiou, Rowan-Robinson & Siebenmorgen 2000; Takagi, Arimoto & Hanami 2003; Siebenmorgen & Krugel 2007), AGN dust tori (Rowan-Robinson & Crawford 1989; Pier & Krolik 1992; Granato & Danese 1994; Efstathiou & Rowan-Robinson 1995; Rowan-Robinson 1995; Nenkova, Ivezic & Elitzur 2002; Dopita et al. 2005; Nenkova et al. 2008; Fritz, Franceschini & Hatziminaoglou 2006; Hönig et al. 2006; Schartmann et al. 2008), and quiescent ('cirrus') galaxies (Rowan-Robinson 1992; Silva et al. 1998; Dale et al. 2001; Efstathiou & Rowan-Robinson 2003; Dullemond & van Bemmel 2005; Piovan, Tantalo & Chiosi 2006; Draine & Li 2006; Efstathiou & Siebenmorgen 2009). Each of these model types involves at least two significant model parameters so there are a great wealth of possible models, particularly as a galaxy SED may be a mixture of all three types.

Rowan-Robinson & Efstathiou (2009) have shown how these models can be used to understand the interesting diagnostic diagram of Spoon et al. (2007) for starburst and active galaxies, which plots the strength of the 9.7 μm silicate feature against the equivalent width of the 6.2 μm PAH feature for 180 starburst and active galaxies with *Spitzer* Infrared Spectrograph (IRS) spectra. Increasing depth of the 9.7 μm silicate feature is, broadly, a measure of the youth of the starburst, because initially the starburst is deeply embedded in its parent molecular cloud. The detailed starburst model of Efstathiou et al. (2000) shows the evolution of the starburst SED through the whole history of the starburst, from the deeply embedded initial phase through to the Sedov expansion phase of the resulting supernovae. However Rowan-Robinson & Efstathiou (2009) did find that there was some aliasing between young starbursts and heavily obscured AGN: the submillimetre data of *Herschel* can help to break this ambiguity, since young starbursts are expected to be much more prominent in the far-infrared and submillimetre than AGN dust tori.

Often, however, we have only limited broad-band data available and in this situation it is more illuminating to use a small number of infrared templates to match the observed infrared colours (e.g. Rowan-Robinson & Crawford 1989; Rowan-Robinson 1992, 2001; Rowan-Robinson & Efstathiou 1993; Rowan-Robinson et al. 2004, Rowan-Robinson et al. 2005, Rowan-Robinson et al. 2008; Franceschini et al. 2005; Polletta et al. 2007; Magdis et al. 2012). A set of just four templates (a quiescent 'cirrus' component, M82- and Arp 220-like starbursts, and an AGN dust torus model) have proved remarkably successful in matching observed *ISO* and *Spitzer* SEDs, including cases where *Spitzer* IRS data are available (Rowan-Robinson et al. 2008; Farrah et al. 2008; Hernan-Caballero et al. 2009).

Following the discussion by Rowan-Robinson & Efstathiou (2009) of the Spoon et al. (2007) *Spitzer*-IRS diagnostic diagram, and our modelling of a sample of 68 HerMES sources (Rowan-Robinson et al. 2010), we have introduced two new templates in our automated fits to far-infrared and submillimetre data: a young ($t = 0$) $A_V = 100$ starburst (our M82 and A220 starburst templates correspond to older starbursts with $A_V = 50$, $t = 40$ Myr, and $A_V = 200$, $t = 30$ Myr, respectively) and a cooler ($\psi = 1$) cirrus model, where ψ is the ratio of the intensity of the radiation field to that in the solar neighbourhood (Rowan-Robinson 1992; Rowan-Robinson et al. 2013; see Section 3 below). Our standard cirrus model corresponds to the ratio of the intensity of the radiation field to that in the solar neighbourhood, $\psi = 5$. In this paper, we explore whether this simple six-template approach works for galaxies detected by the SPIRE array (Griffin et al. 2010) on *Herschel*, and what additional infrared components may be present. We apply the method to a large sample of *Herschel* sources, ∼1000 galaxies, in an area of the sky where we have a wealth of ancillary data at optical, near-, mid- and far-infrared wavelengths. We use physical models derived from radiative transfer codes to gain a deeper understanding of the evolutionary status of the infrared galaxies and the balance between starburst and quiescent phases. Submillimetre wavelength data reveal the presence of colder dust than is detected at far-infrared wavelengths.

Another key phenomenon in understanding submillimetre galaxies is gravitational lensing. Negrello et al. (2007, 2010) have shown that a significant fraction of bright 500 μm galaxies are lensed (see also Wardlow et al. 2013). In this paper, we explore whether anomalous excess submillimetre radiation in fainter galaxies may be due to lensing. Detailed SED modelling is needed to distinguish cold dust from the effects of gravitational lensing.

A flat cosmological model with $\Lambda = 0.7$, $h_0 = 0.72$ has been used throughout.

2 SELECTION OF SAMPLE WITH HIGH QUALITY FLUX-DENSITIES AT 24, 250, 350 AND 500 μm

In this analysis, we have focused on the HerMES[1] (Oliver et al. 2012) SCAT catalogue (Wang et al. 2014) in the SWIRE-Lockman area (Lonsdale et al. 2003), where we have optical and 3.6–160 μm *Spitzer* photometry, photometric redshifts, and infrared template fits from the SWIRE photometric redshift catalogue (Rowan-Robinson et al. 2008, 2013).

Our starting point is the HerMES SPIRE (SCAT) 500 μm catalogue (Wang et al. 2014) with sources detected at 500 μm without using any prior information from the other SPIRE bands (i.e. 'blind' 500 μm catalogue). We choose this starting-point, rather than the XID catalogue of Roseboom et al. (2010), because we want to reconsider the process of associating SPIRE sources with *Spitzer* 24 μm sources. There are 2970 sources in the HerMES-Lockman area that are detected at better than 5σ at 500 μm. Here, we are using the estimated total error, which includes the contribution of confusion noise, ∼6.8 mJy beam^{-1} (Nguyen et al. 2010). The process of building a band-merged catalogue begins by looking for associations with 5σ 350 μm SCAT sources, using a search radius of 30 arcsec. The SPIRE beam full width at half-maximum is 18.2, 25.2, 36.3 arcsec at 250, 350, 500 μm, respectively (Griffin et al. 2013). 2709 sources found associations and we shall ignore the 261 sources (8.7 per cent) which did not find associations with well detected 350 μm sources. Some of these may be high-redshift 'red' sources (Dowell et al. 2014) while others may be combinations of two or more fainter 500 μm sources. We note that 122 did find associations with 350 μm sources detected at 4–5σ but we have not pursued these further here. Of these 2709 5σ 350–500 μm sources, 1335 lie in the area covered by the *Spitzer* SWIRE survey (Fig. 1) and it is this latter sample that we focus on in this paper.

We next associated the 1335 350–500 μm sources in the SWIRE area with 250 μm sources detected at better than 5σ, using a search

[1] HerMES.sussex.ac.uk

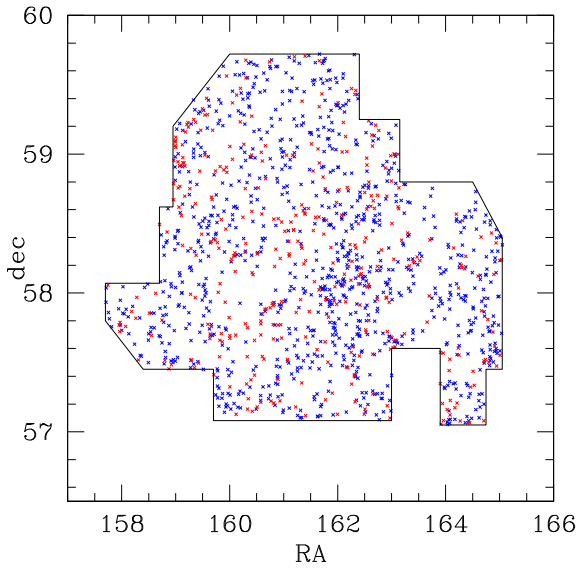

Figure 1. The region of overlap of the HerMES SPIRE survey area and the SWIRE photometric redshift survey in the Lockman Hole area. HerMES 500 μm sources associated with SWIRE sources in blue, unassociated sources in red.

radius of 30 arcsec from the 350 μm position. 879 found associations, and a further 163 found associations with 250 μm sources detected at 4–5σ. The remaining 293 350–500 μm sources we regard as undetected at 250 μm. Fig. 2 (left) shows the distribution of separations between SCAT 250 and 350 μm sources. Most associations have separations <10 arcsec (97 per cent are within 20 arcsec) and associations with separations in the range 20–30 arcsec should perhaps be treated with caution.

Finally, we associated the 1335 350–500 μm sources with the SWIRE Photometric Redshift Catalogue (Rowan-Robinson et al. 2008, 2013), using a 20 arcsec search radius from the 250 μm position (or 350 μm if no 250 μm detection), and requiring a 24 μm detection brighter than 100 μJy, above which the SWIRE 24 μm catalogue is ∼95 per cent reliable. The 24 μm 70 per cent completeness limit is ∼300 μJy in the Lockman field (90 per cent at 400 μJy).

The SWIRE Photometric Redshift Catalogue contains over 1 million galaxies covering 49 deg^2 of sky, including 7.53 deg^2 in Lockman, which had been surveyed at 3.6–160 μm by *Spitzer* and at *ugrizJHK* in ground-based surveys. Photometric redshifts were determined from *ugrizJHK* and 3.6, 4.5 μm photometry (with up to 13 photometric bands available in the Lockman area) and the 5.8–160 μm data were fitted with infrared templates. These allowed prediction of fluxes at submillimetre wavelengths. If more than one SWIRE source is associated with a HerMES SCAT source, the source with the highest predicted 450 μm flux from the SWIRE Photometric Redshift Catalogue is selected. Thus, the redshift and the 5.8–160 μm flux information are being used to select the best association. Inevitably there will be cases where the submillimetre flux should be assigned to more than one source because of the effects of confusion, and here a more sophisticated treatment would require comparison of multiwavelength maps. However, we believe our approach gives more reliable results than assigning flux purely on the basis of the 24 μm flux, as in Roseboom et al. (2010). We found a total of 967 SWIRE associations, 73 per cent of the 1335 total. For 13 sources, two SPIRE sources selected the same 24 μm source and in these cases we deleted the weaker 500 μm source from the list. We expect the bulk of the 368 unassociated sources to be at redshift >1.5, given the SWIRE selection function. Fig. 3 shows 500 μm flux-density versus 24 μm flux-density for the associated sources. The 24 μm limit of 100 mJy has little effect on the sample selection. Fig. 4 (left) shows the 250–350–500 μm colour diagram with the loci of the infrared templates overplotted. The lower SNR 250 μm sources tend to have bluer SPIRE colours and be at higher redshift.

This is essentially a 500 μm selected sample, with the additional requirements of multiwavelength associations. The reason for making the selection at 500 μm is to maximize the number of sources with photometry at all three SPIRE wavelengths, since the focus of this paper is on SED modelling. Our requirement of association with a SWIRE 24 μm source discriminates against sources with $S(500)/S(24) > 200$, and our requirement of an entry in the SWIRE Photometric Redshift Catalogue discriminates against sources with $z > 1.5$ (see fig. 14, left, of Rowan-Robinson et al. 2008). Selection at 500 μm favours galaxies with cooler dust, than say selection at 70 or even 250 μm.

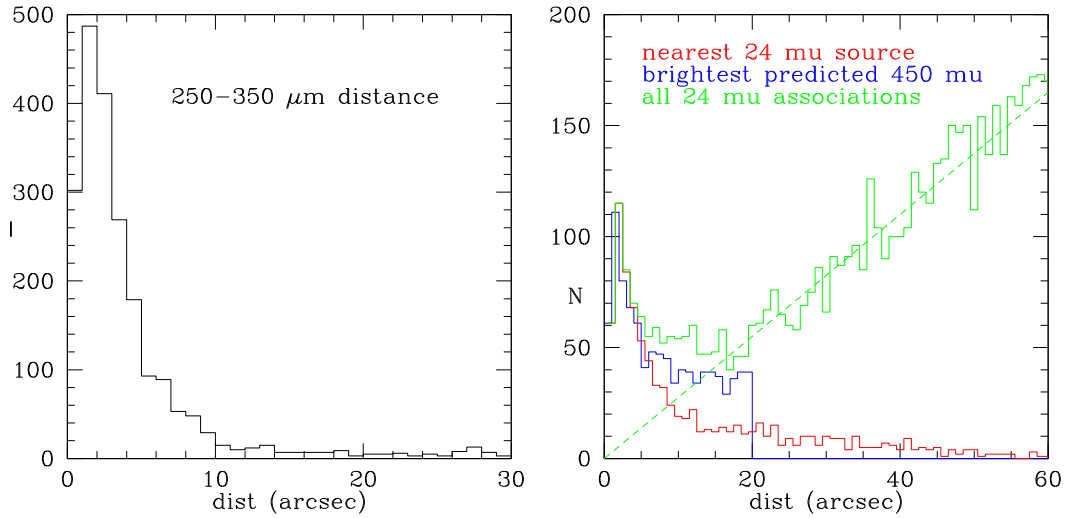

Figure 2. Left hand: distribution of separations between SCAT 250 and 350 μm associations. Right hand: distribution of separations between SWIRE and SPIRE sources for nearest 24 μm source (red), all 24 μm sources (green), and the brightest predicted 500 μm source (blue).

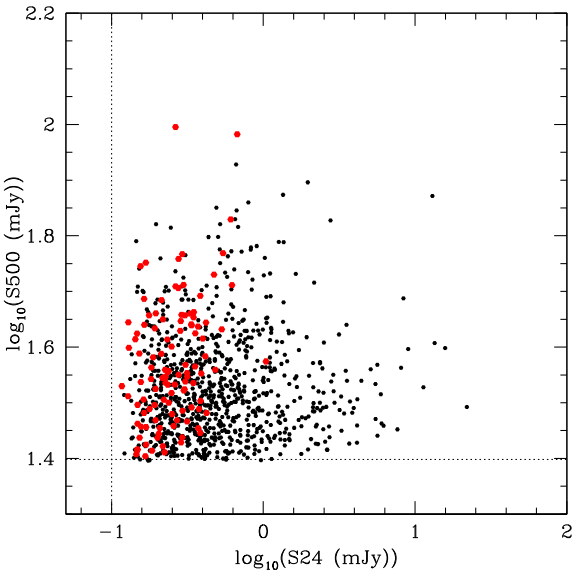

Figure 3. *S*500 versus *S*24 for Lockman-SCAT sources (red points: lens candidates, see Section 4). The dotted lines indicate the 500 μm sensitivity limit of 25 mJy and the 24 μm cutoff of 100 μJy.

Fig. 2 (right) shows the distribution of separations between SPIRE and SWIRE sources for the nearest 24 μm source (in red), for all 24 μm sources, and for our adopted associations with the SWIRE 24 μm source within 20 arcsec with the brightest predicted 500 μm flux. The green distribution shows the linear increase at large separations characteristic of random associations. Our procedure ensures that the incidence of chance associations is kept low, but will be higher where the separation is >10 arcsec. Although our 500 μm flux-density selection limit is set at five times the total error, including confusion noise, it is possible that a few 500 μm sources are in fact blends of two or more fainter sources (see further discussion of the issues of confusion and misassociation in Section 5).

3 SEDS OF *HERSCHEL* GALAXIES

We first ran an automated infrared SED-fitting code to the 3.6–500 μm (10 photometric band) data for all 967 HerMES-SWIRE sources in Lockman, using the six infrared templates discussed in Section 1. Fig. 4 (right) shows a histogram of the reduced $\chi^2_{\rm ir}$ for these fits. The fits are satisfactory except that there is a long tail of high $\chi^2_{\rm ir}$ values. Fits where $\chi^2_{\rm ir} > 5$, of which there are 69 out of the 967 total, we regard as requiring further explanation, either in terms of photometry problems, a need for additional infrared templates, or as indicating the presence of gravitational lensing.

However, even where $\chi^2_{\rm ir} < 5$, we regard a solution where the luminosity in the optically thin 'cirrus' component is greater than the total luminosity in starlight (after correction for extinction), as unphysical and requiring further scrutiny.

We have plotted here (Figs 5–14, 18–23) the individual SEDs of a large sample of the 967 HerMES-SWIRE sources in Lockman, 259 sources in total. These are divided into four distinct subsamples: (1) sources with $\chi^2_{\rm ir} > 5$ and at least 10 optical–NIR (0.36–4.5 μm) photometric bands, (2) sources with $\chi^2_{\rm ir} < 5$ and at least 12 optical–NIR photometric bands, (3) sources with 10 photometric bands and $\chi^2_{\rm ir} < 5$ but $L_{\rm cirr} > L_{\rm opt}$, (4) candidate gravitational lenses (see Section 4). Approximately half of the SED plots are not shown here but given in the online supplementary material.

The individual SED modelling follows the methodology of Rowan-Robinson et al. (2005, 2008), but with some new features. Optical and near-infrared (NIR) data are fitted with one of six galaxy templates and two QSO templates, with the extinction A_V as a free parameter. Infrared and submillimetre data are fitted with a combination of seven infrared templates (three cirrus models ($\psi = 5$, 1, 0.1, see below), one of three starburst models (M82, A220, and a young starburst), and an AGN dust torus model). The 'cool' cirrus template ($\psi = 1$) and 'cold' cirrus template ($\psi = 0.1$), and the young starburst template are brought in following the demonstration by Rowan-Robinson et al. (2010) of the need for these templates when modelling *Herschel* sources. Most SEDs are well fitted by only one or two infrared templates, and in no case is more than four templates used.

Spectroscopic redshifts have been indicated in the SED plots by showing four decimal places. The accuracy of the photometric

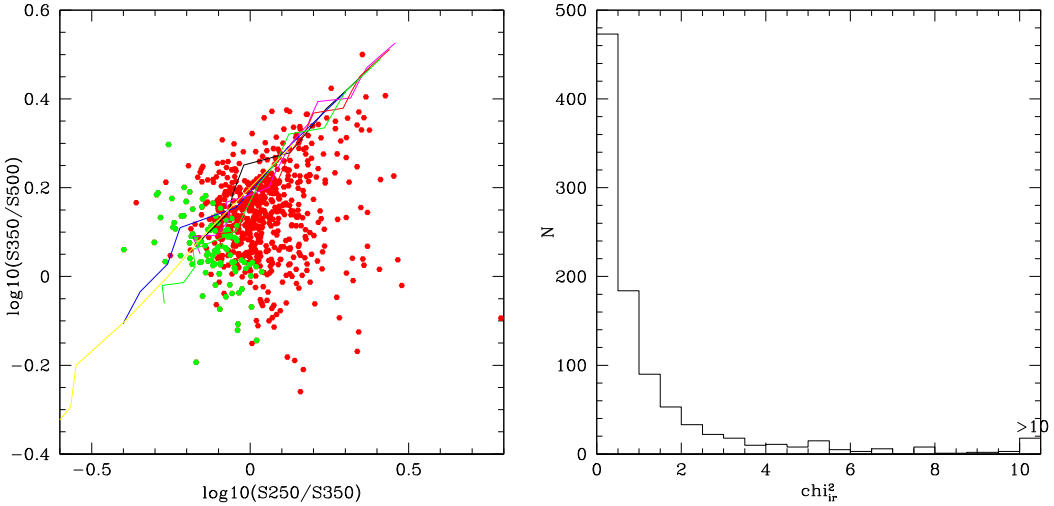

Figure 4. Left hand: 250–350–500 μm colour–colour diagram for SCAT Lockman sources with 5σ detections at 250 and 350 μm, and which are also associated with SWIRE 24 μm sources (red: >5σ at 250 μm; green: 4–5σ at 250 μm. Coloured loci are for different templates, with $z = 0$ at top right, $z = 4$ at bottom left. Right hand: histogram of reduced $\chi^2_{\rm ir}$ from our automated six-template fit to our sample of 967 HerMES-Lockman galaxies.

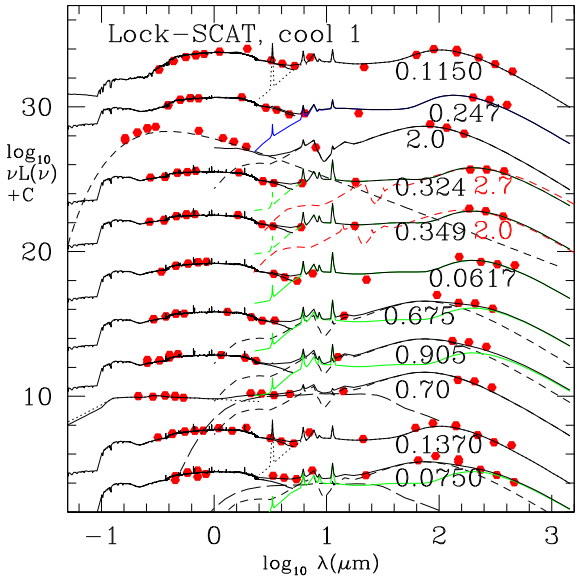

Figure 5. SEDs for SWIRE-Lockman galaxies with at least 10 optical–NIR photometric bands and with $\chi^2_{\rm ir} > 5$. Cool cirrus models ($\psi = 1$) are shown in blue, cold cirrus models ($\psi = 0.1$) in green. Lens models are shown as red broken curves, with associated redshift of lensed galaxy in red. Black dotted curves are cirrus ($\psi = 5$) or M82 starbursts, black dashed curves are Arp 220 starbursts and black long-dashed curves are AGN dust tori. Where a lensed galaxy is also shown with a cirrus template fit, the latter has been rejected as physically implausible because $L_{\rm cirr} > L_{\rm opt}$.

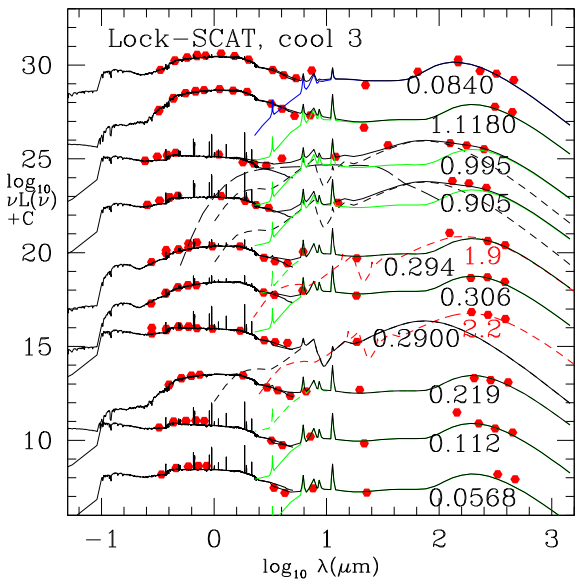

Figure 6. SEDs for SWIRE-Lockman 10-band galaxies with $\chi^2_{\rm ir} > 5$. Colour-coding as in Fig. 5.

redshifts is ∼4 per cent in (1+z) for most of the galaxies, where six or more photometric bands are available (Rowan-Robinson et al. 2013). The full χ^2 distribution for each photometric redshift estimate is given in the SWIRE Photometric Redshift Catalogue. The optical galaxy templates are those of Rowan-Robinson et al. (2008) and are shown at full resolution in the SED plots.

While the four standard infrared templates work well for many sources, the 350 and 500 μm fluxes often require the presence of

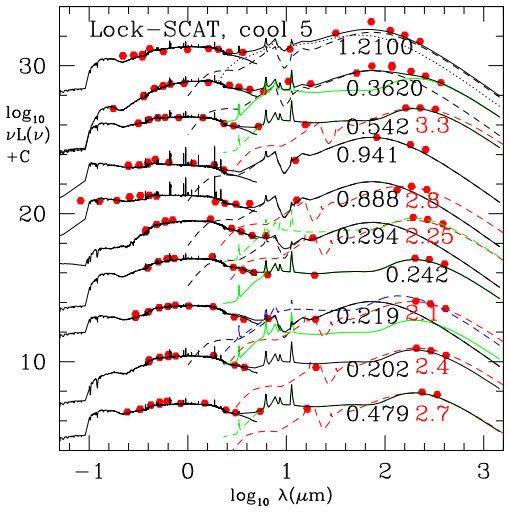

Figure 7. SEDs for SWIRE-Lockman 10-band galaxies with $\chi^2_{\rm ir} > 5$.

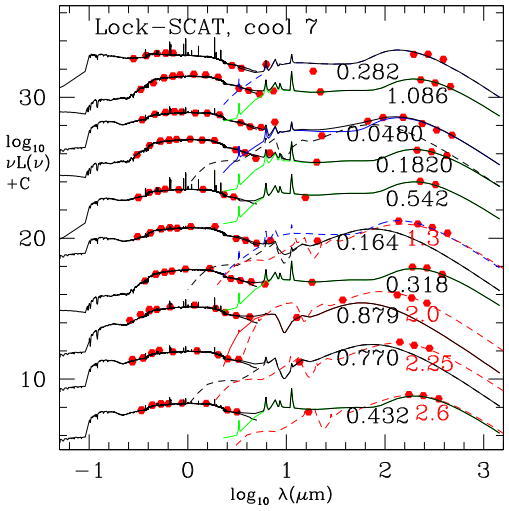

Figure 8. SEDs for SWIRE-Lockman 10-band galaxies with $\chi^2_{\rm ir} > 5$..

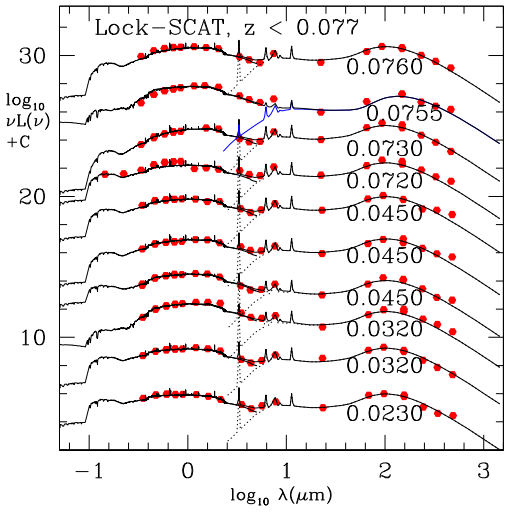

Figure 9. SEDs for SWIRE-Lockman galaxies with at least 12 optical–NIR photometric bands and with $z < 0.077$. Photometric redshifts are indicated with only three significant figures. Colour-coding as in Fig. 5.

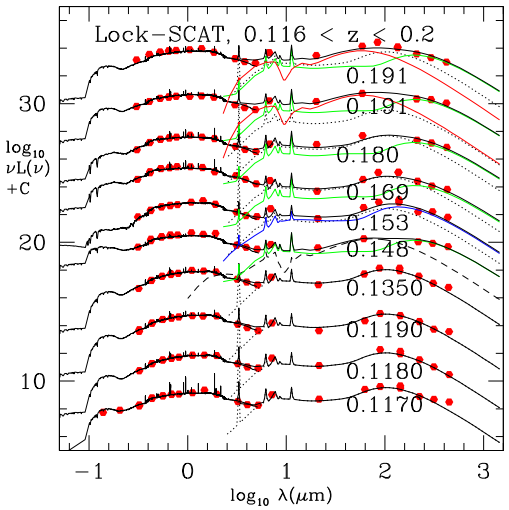

Figure 10. SEDs for SWIRE-Lockman 12-band galaxies with $0.116 < z < 0.2$. Solid red curves are young starbursts.

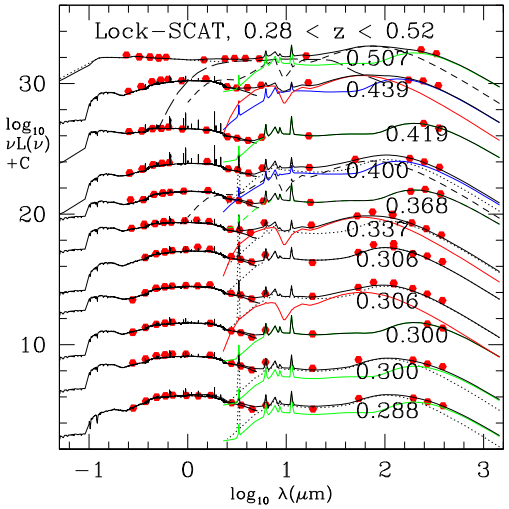

Figure 11. SEDs for SWIRE-Lockman 12-band galaxies with $0.28 < z < 0.52$.

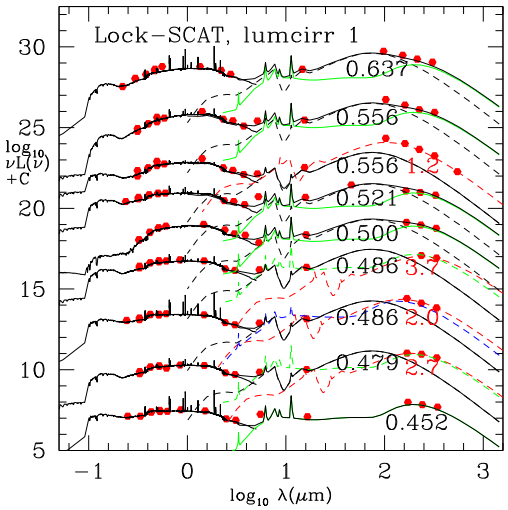

Figure 13. SEDs for SWIRE-Lockman galaxies with $L_{\rm cirr} > L_{\rm opt}$. Colour-coding as in Fig. 5.

colder dust than is incorporated into our four basic templates. The two new cirrus templates used here are taken from the range of optically thin interstellar medium ('cirrus') templates developed by Rowan-Robinson (1992) and Efstathiou & Rowan-Robinson (2003). The key parameter determining the temperature of the dust grains for optically thin emission is the intensity of the radiation field, which we can characterize by the ratio of intensity of radiation field to the local Solar Neighbourhood interstellar radiation field, ψ. The standard cirrus template corresponds to $\psi = 5$, and this is the value used by Rowan-Robinson (1992) to fit the central regions of our Galaxy. $\psi = 1$ corresponds to the interstellar radiation field in the vicinity of the Sun. We also find that some galaxies need a much lower intensity radiation field than this, with $\psi = 0.1$. The corresponding grain temperatures in the dust model of Rowan-Robinson (1992) are given in table 1 of Rowan-Robinson et al. (2010). For the two new templates, the ranges of dust grain temperatures for the different grain types are 14.5–19.7 K and 9.8–13.4 K,

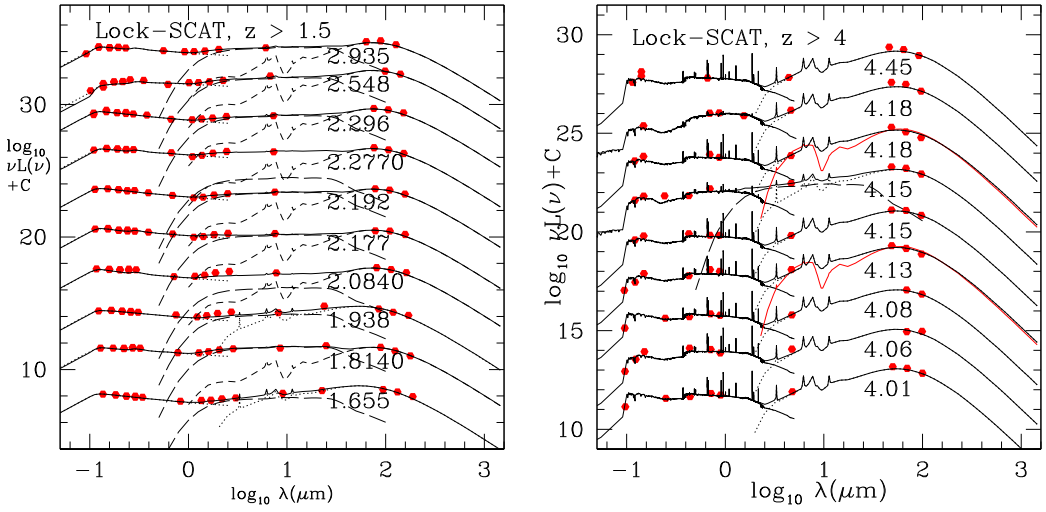

Figure 12. Left: SEDs for SWIRE-Lockman 12-band galaxies with $z > 1.5$. Right: SEDs for seven-band SWIRE-Lockman galaxies with $z > 4$.

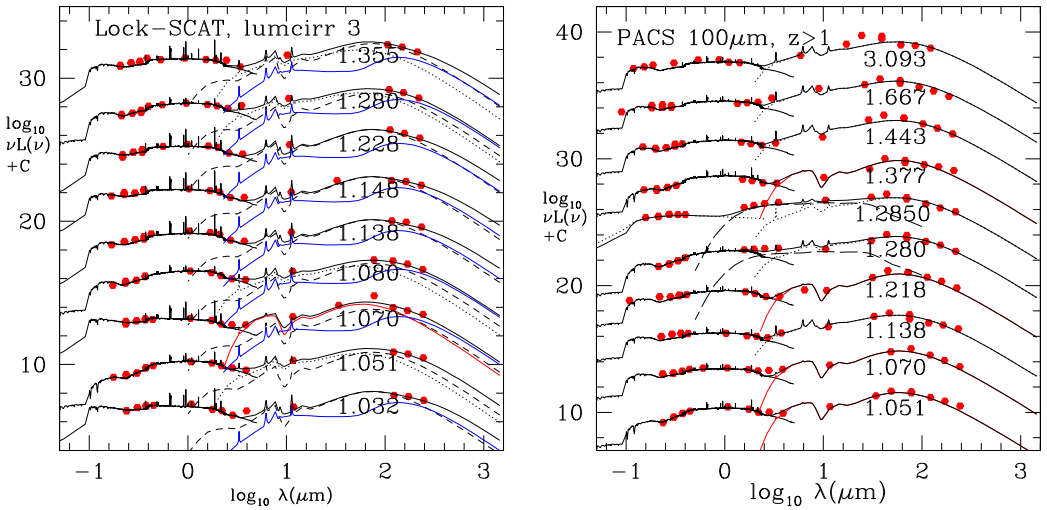

Figure 14. Left hand: SEDs for SWIRE-Lockman galaxies with $L_{\rm cirr} > L_{\rm opt}$. Right hand: SEDs for SWIRE-Lockman galaxies with redshifts >1, determined from at least seven photometric bands, and PACS 100 and 160 μm detections.

respectively. Full details of the templates used are given in a readme page.[2]

The need for cooler dust templates can also be seen clearly in a plot of $S(500)/S(24)$ versus redshift (Fig. 16), in which the predictions of different templates are shown. At $z < 1$, a significant fraction of galaxies require colder dust than the standard cirrus model. Hints of this population were seen at $z < 0.4$ in the plot of *ISO* 175/90 μm flux ratio versus redshift (fig. 23) of Rowan-Robinson et al. (2004). Symeonidis et al. (2009) plotted a very similar figure, 160/70 μm flux ratio versus redshift, for *Spitzer* data. They interpreted this as implying strong evolution in the cold dust component. The need for cooler dust was also seen in the *Planck* study of nearby galaxies (Ade et al. 2011).

3.1 Problematic sources with $\chi^2_{\rm ir} > 5$

First, we show the SEDs of problematic sources with $\chi^2_{\rm ir} > 5$ in the automated six-template fit, for sources with redshifts determined from 10 optical and NIR photometric bands (Figs 5–8). Most have $\log(S500/S24) > 2$ and $z < 1$. For over half the sources, the introduction of the cold cirrus template ($\psi = 0.1$) solves the problem of the poor fit. In many cases none of our existing templates can match the observed SEDs. Since it is implausible to postulate emission from cold dust with a luminosity exceeding that of the illuminating starlight, the association of the submillimetre emission with the chosen SWIRE galaxy must be incorrect. A possible explanation is provided by galaxy lensing. In several cases, we have indicated fits to the submillimetre data with an Arp 220 starburst model at a higher redshift than that of the SWIRE galaxy.

3.2 Sources with good infrared template fits

We now show the SEDs for 69 sources with redshifts determined from at least 12 optical–NIR photometric bands and with $\chi^2_{\rm ir} < 5$ (Figs 9–12). In almost all cases, the optical and NIR data are well fitted by the galaxy or QSO templates and the photometric redshifts look very credible. The infrared template fits to $\lambda > 4.5$ μm data also look good. 20 galaxies need a cold cirrus component and 3 are gravitational lens candidates. The latter are cases where in the automatic fitting the submillimetre data are fitted with a cirrus component with luminosity greater than that of the starlight, so a physically implausible fit despite the acceptable $\chi^2_{\rm ir}$.

The requirement of 12 optical and NIR bands biases the sample against high redshifts, so we also show the SEDs for sources with seven photometric band redshifts, $\chi^2_{\rm ir} < 5$, and $z > 4$ (Fig. 12, right).

We also incorporated photometry from the PACS data (Poglitsch et al. 2010). The Lockman-SWIRE field was observed by HerMES (AOT Set no. 34; Oliver et al. 2012) using the SPIRE/PACS parallel mode. Maps were reduced using the UNIMAP software (Piazzo et al. 2012). Photometry was estimated by constructing a 'beam' from stacking the PACS map at the location of all 967 sources and fitting this beam to the location of each source (this does not include a correction for the extended PACS beam). We found 136 with $S(100) > 80$ mJy, or $S(160) > 120$ mJy. These thresholds (corresponding approximately to 3σ detections and >95 per cent reliability) were selected after comparison with SWIRE 70 and 160 μm fluxes, with predictions from our template fits, and from examination of individual SEDs. When these 136 sources lie in our SED plots (Figs 5–14), the PACS 100 and 160 μm fluxes have been included and these are generally consistent with the SWIRE 70 and 160 μm fluxes and the fitted models. We have also shown SEDs for 10 sources with PACS 100 and 160 μm fluxes and $z > 1$ (Fig. 14, right). The PACS fluxes generally agree well with the fitted models.

3.3 Problematic sources with $L_{\rm cirr} > L_{\rm opt}$

Figs 13 and 14 (left) show SEDs for sources with at least 10 optical–NIR photometric bands, and with $\chi^2_{\rm ir} < 5$, but where $L_{\rm cirr} > L_{\rm opt}$ in the automated six-template fits. While some can be fitted adequately by including a cold cirrus template without violating the $L_{\rm cirr} \leq L_{\rm opt}$ requirement (and all at $z > 0.92$), many require a lensing model to fit the submillimetre data.

In summary, the total number of candidate lenses from Figs 5–14 is 36. Is there an alternative explanation to lensing for these galaxies with excessive submillimetre radiation? Cold cirrus is not an option for these lensing candidates because the luminosity in cold dust would exceed that in starlight. Our association procedure ensures that there is no other more likely 24 μm association for

[2] http://astro.ic.ac.uk/public/mrr/swirephotzcat/templates/readme

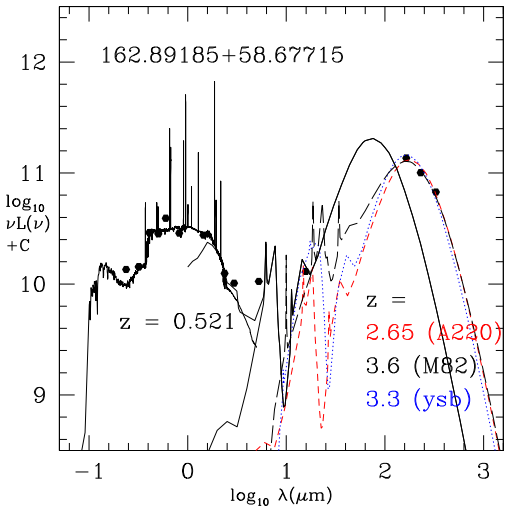

Figure 15. SEDs for a candidate lensed galaxy (bottom galaxy in Fig. 11, right) with photometric redshift determined from 12 photometric bands, showing fits with Arp 220 (dashed), M82 (dash–dotted) and young starburst (dotted) templates.

the submillimetre source. Any other association would have an even worse SED-fitting problem. It is possible that in some cases we have a chance association of a $z \sim 0.5$ SWIRE galaxy whose true submillimetre output is weak with a high-redshift luminous submillimetre galaxy which is undetected in the SWIRE survey. We discuss in Section 5 the probability for this to happen.

The lens model SED fits have an ambiguity about which starburst template to use. All fits shown use the Arp 220 template, but Fig. 15 illustrates ambiguity in redshift for a lensed galaxy from using the M82 or young starburst templates. The values of $(1 + z_{\rm lens})$ that we are quoting need to be multiplied by 1.25 if a young starburst model is preferred or by 1.36 if an M82-like starburst is preferred.

We now use these 36 candidate lenses to define regions of colour–redshift space to identify a further 73 lensing candidates from the sources with less than 10 optical–NIR photometric bands.

4 USING COLOUR–REDSHIFT DIAGRAMS TO SELECT LENSING CANDIDATES

Our SED modelling of problematic sources with 10-band photometric redshifts has identified 36 candidate lensed galaxies, in which the optical and NIR data define the lensing galaxy and the submillimetre data are due to the background lensed galaxy. We now explore whether we can use colour–redshift plots to characterize lensing candidates amongst fainter sources, which generally have fewer photometric bands available.

The 36 galaxies occupy a rather well defined area in the plot of $\log_{10}S500/S24$ versus redshift (Fig. 16), which cannot be reached by our infrared templates. In addition, Wardlow et al. (2013) have shown that gravitational lens candidates have well-defined 250–350–500 μm colours. Fig. 17 (left) shows $\log_{10}S500/S350$ versus redshift for SCAT Lockman sources, with lens candidates shown in red. The Wardlow et al. criterion, $S350/S500 < 1.8$ does indeed include all our lensing candidates selected on the basis of their SEDs. We do not try to use the 250 μm flux since some of our sources are not detected at 250 μm.

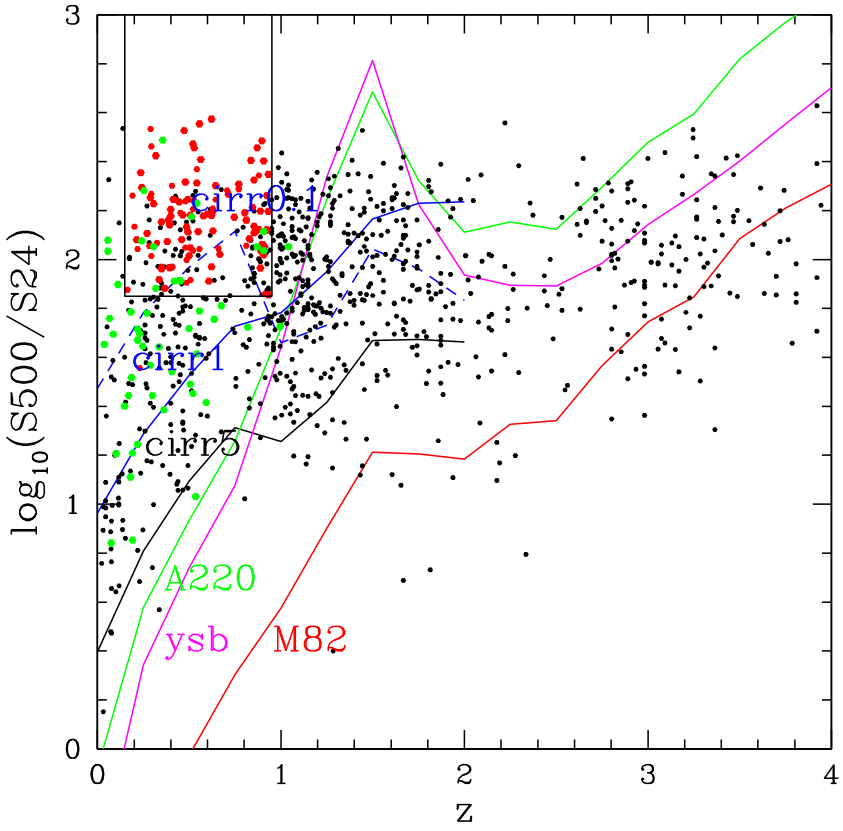

Figure 16. 500/24 μm flux ratio versus redshift for SCAT Lockman sources with 5σ detections at 350 and 500 μm, and which are also associated with SWIRE 24 μm sources (filled black circles). Filled red circles: 109 lensing candidates; green filled circles: 50 galaxies requiring cold dust template ($\psi = 0.1$).

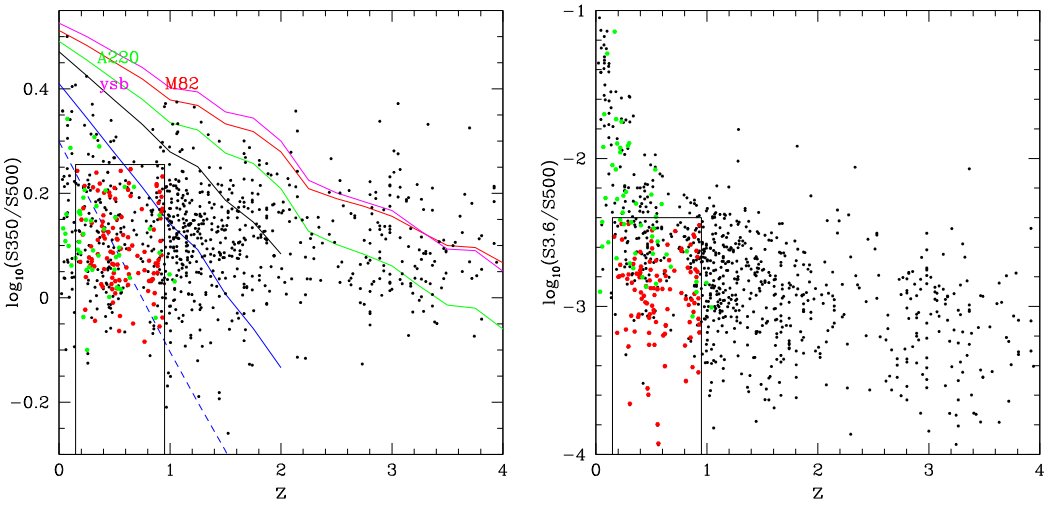

Figure 17. Left: 350–500 μm colour versus redshift for SCAT Lockman sources with 5σ detections at 350 and 500 μm, and which are also associated with SWIRE 24 μm sources. Lensed sources shown in red, galaxies requiring cold dust in green. Right: 3.6/500 μm flux-ratio versus redshift for SCAT Lockman sources with 5σ detections 350 and 500 μm and which are also associated with SWIRE 24 μm sources.

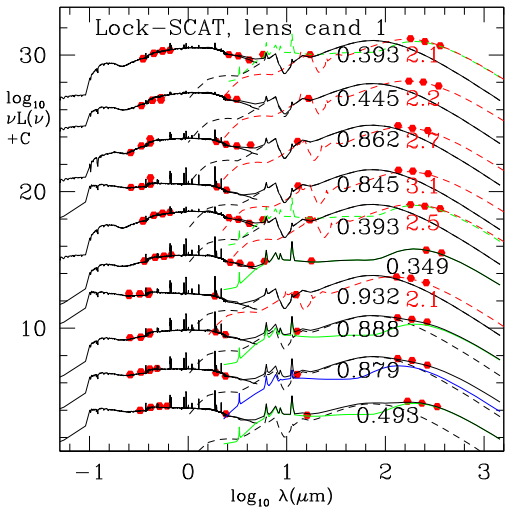

Figure 18. SEDs for SWIRE-Lockman galaxies with <10 photometric bands which are lens candidates according to the colour–redshift criteria of Section 4.

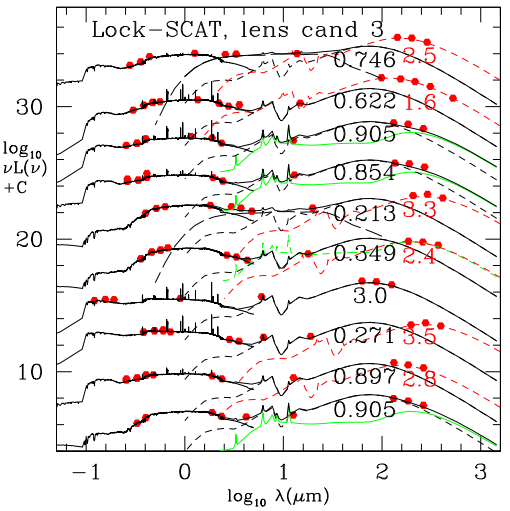

Figure 19. SEDs for SWIRE-Lockman galaxies with <10 photometric bands which are lens candidates according to the colour–redshift criteria of Section 4.

To capture the $L_{\rm cirr} > L_{\rm opt}$ indication of lensing we have plotted $\log_{10}S3.6/S500$ versus redshift (Fig. 17, right), with lensing candidates on the basis of their SEDs in red. Again the lensing candidates occupy a well-defined area of this diagram.

We can now define criteria which lensed candidates in our sample are likely to satisfy: $0.15 < z < 0.95$, $\log_{10}(S3.6/S500) < -2.40$, $S350/S500 < 1.8$, and $\log_{10}(S500/S24) > 1.85$. Here, we are assuming that the redshift determined from optical and NIR photometry applies to the lensing galaxy. We have modelled the SEDs of all the 117 galaxies satisfying all three criteria with redshifts based on less than 10 photometric bands (Figs 18–23). Of these, 44 could be fitted with our standard 7 templates and without violating $L_{\rm cirr} \leq L_{\rm opt}$ (21 of these involve cold dust). The remaining 73 are lensing candidates. Of the 117 sources satisfying our colour constraints, 63 per cent are lensing candidates while 18 per cent require cold dust. In total we have 109 lensing candidates, based on their SEDs, out of our total sample of 967 Lockman-SCAT-SWIRE sample (11.3 per cent), or 8 per cent of our Lockman-SCAT 500+350 μm sample. These include the Wardlow et al. (2013) confirmed lens HLock04 and lensing candidate HLock06, which fall in the SWIRE area. HLock01 is not in our catalogue but would satisfy our lensing criteria. The stellar masses of our candidate lensing galaxies most lie in the range $\log_{10}M_*/{\rm M}_\odot = 10.5$–$11.5$, with a mean value 11.0.

Our lensing criteria could be on the conservative side, because in some cases submillimetre emission could be lensed even though there is an acceptable fit to the SED from a non-lensed model. Some of the lensing candidates will be chance associations of a high-redshift submillimetre galaxy with a lower redshift 24 μm galaxy (see the next section) and this can only be resolved by submillimetre intereferometric imaging.

5 CONFUSION AND CHANCE ASSOCIATIONS

The restriction to 5σ detections should ensure that most of our sources are distinct independent galaxies. The source-density of our sample corresponds to one source per 36 beams, so the probability

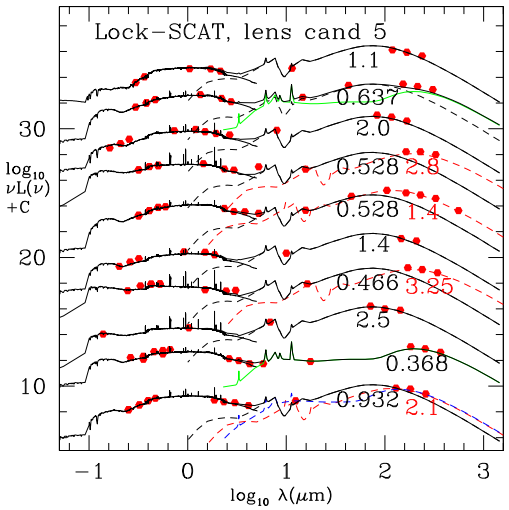

Figure 20. SEDs for SWIRE-Lockman galaxies with <10 optical–NIR photometric bands which are lens candidates according to the colour–redshift criteria of Section 4. Colour-coding as in Fig. 5.

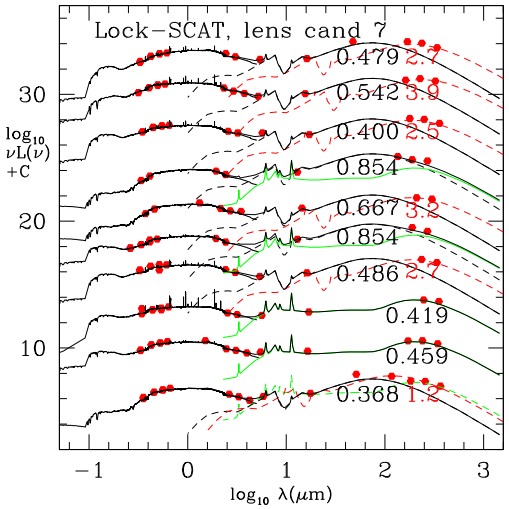

Figure 21. SEDs for SWIRE-Lockman galaxies with <10 photometric bands which are lens candidates according to the colour–redshift criteria of Section 4.

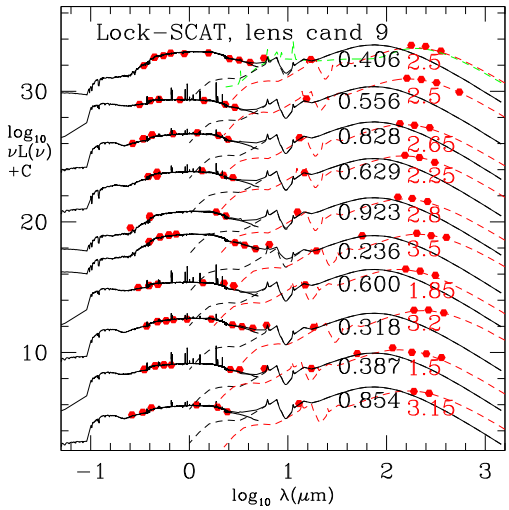

Figure 22. SEDs for SWIRE-Lockman galaxies with <0 photometric bands which are lens candidates according to the colour–redshift criteria of Section 4.

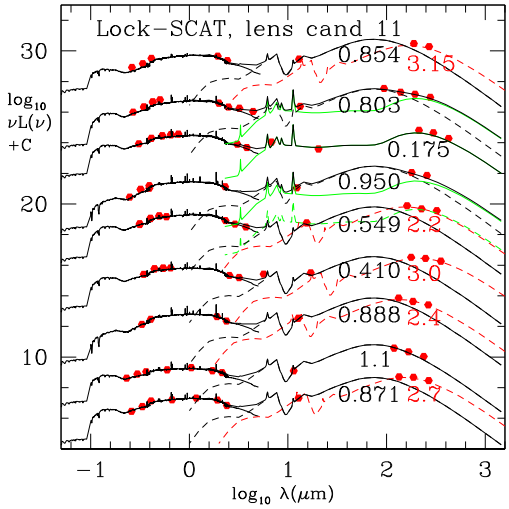

Figure 23. SEDs for SWIRE-Lockman galaxies with <10 photometric bands which are lens candidates according to the colour–redshift criteria of Section 4.

of a source being a blend of two fainter sources in the beam is low, ignoring correlations. However, the limited *Herschel* resolution, combined with the high source-density of *Spitzer* 24 μm sources, means that the issue of incorrect association between SPIRE and SWIRE sources is a serious one. This is especially important when we are claiming to identify the presence of unusually cold dust or of gravitational lenses from anomalous SEDs.

For our 109 gravitational lens candidates and the 50 sources whose SEDs we have claimed require the presence of cold dust, we have therefore very carefully examined the regions around the SPIRE sources for alternative associations. We have looked for all additional 24 μm associations (with $S24 > 100$ mJy) within 20 arcsec of the SPIRE position, which are either closer than our preferred association or are brighter at 24 μm (or both). 22 of the 109 lens candidates yielded a total of 25 alternative associations, while 8 of the 50 galaxies requiring cold dust yielded a total of 10 alternative associations. The remaining 87 lens candidates and 42 cold dust galaxies did not have an alternative 24 μm association.

We have modelled the SEDs of these 35 sources, assuming the 250–500 μm flux belongs to these alternative associations rather than our preferred association based on the predicted 450 μm flux. Of the 25 lens candidate alternative associations, 20 still needed a lensing model, 5 did not. Thus for 95 per cent of our lens candidates, there is no alternative to a lensing model, though there may be ambiguity about which galaxy is the lens in some cases. For ∼5 per cent of our lens candidates, the choice of a lensing model may be due to the wrong association. Clearly, there is a need for submillimetre interferometry to confirm the reality of these lensing candidates, and to clarify which 24 μm source is the lens in the ambiguous cases.

Of the 10 cold dust galaxy alternative associations, 6 require a lensing model, 1 requires a cold dust component, and 3 do not require a lensing model or cold dust component. We see from Figs 16 and 17 that some of the cold dust galaxies occupy the same regions of the colour–redshift diagrams as the lensing candidates, so there is ambiguity in the interpretation of their anomalous SEDs. However, most cold galaxies lie outside the zones occupied by

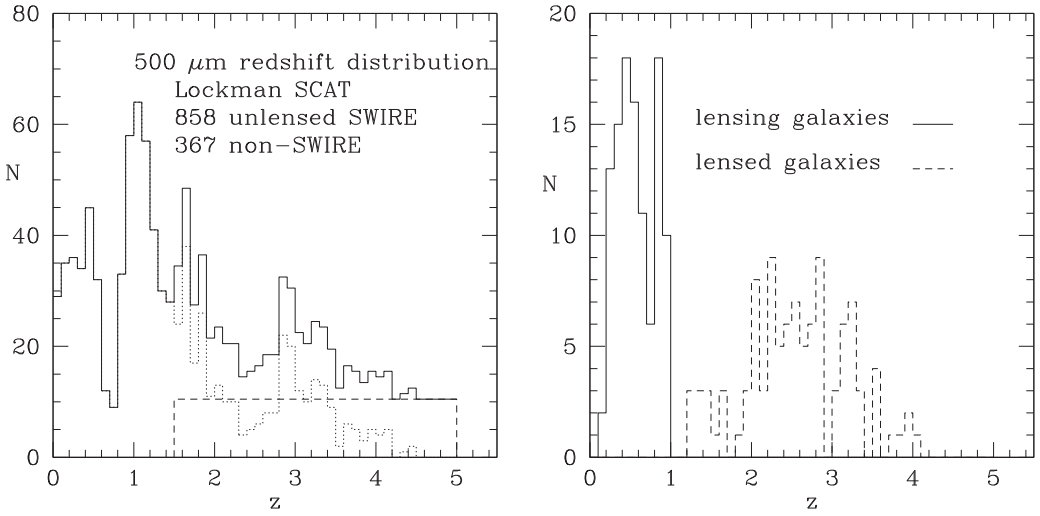

Figure 24. Left: redshift distribution for unlensed SCAT 500 μm sources in Lockman. Sources not associated with SWIRE galaxies have been shown uniformly distributed between $z = 1.5$ and $z = 5$. Right: redshift distribution for SCAT 500 μm lensing galaxies (solid locus) and for corresponding lensed galaxies (dashed locus).

lensing candidates in Figs 16 and 17 (right), so there is a reasonably clear separation in the colours of lensing candidates and cold galaxies. If the luminosity in the submillimetre component is less than the optical–NIR starlight luminosity, we have assumed a cold dust interpretation, but a low-luminosity lensed galaxy interpretation cannot be excluded. Again submillimetre interferometry is the key to confirming the correctness of the cold dust interpretation, since these would be expected to be unusually extended because ψ is a measure of surface brightness, so for a given luminosity lower ψ implies a larger diameter for the dust cloud.

We also need to estimate the probability that the association of a $z = 0.15$–0.95 SWIRE galaxy with a 500 μm source is spurious because the submillimetre source is in fact a background high-redshift galaxy without a SWIRE detection, which is associated with a foreground SWIRE galaxy by chance. For each of the 368 500 μm sources which did not find a 24 μm association, which are our candidate background high redshift galaxies, we estimate the probability of a chance association with a $z = 0.15$–0.95 SWIRE 24 μm galaxy, requiring that our lensing criteria (Section 4) be satisfied. We estimate 24 chance associations within the 7.5° Lockman-HerMES area, so ∼22 per cent of our lensing candidates could be chance associations of a 24 μm galaxy with a background high-z 500 μm galaxy.

Finally, we should consider whether the attribution of sources as lensing candidates could be due to catastrophic outliers in the photometric redshift estimate. Of the 109 lensing candidates, 65 have redshifts determined from at least nine photometric redshift bands, for which the probability of a catastrophic outlier is <1 per cent (Rowan-Robinson et al. 2013); 35 have redshifts determined from five to eight bands, for which the probability of a catastrophic outlier is 1–3 per cent, 8 have redshifts determined from 3 to 4 bands, for which the probability of a catastrophic outlier is 10–20 per cent; and 1 have redshifts determined from two bands, which are highly uncertain. So catastrophic outliers could account for up to five of the lensing candidates. From the SEDs, all the photometric redshifts look plausible.

To summarize, we estimate that ∼5 per cent of the candidate lensed galaxies could be due to catastrophic photometric redshift outliers, ∼5 per cent could be cases where the wrong SWIRE association has been chosen, and ∼20 per cent are likely to be chance associations of a high-redshift 500 μm galaxy with a lower redshift 24 μm galaxy.

6 DISCUSSION

Fig. 24 (left) shows the redshift distribution for the 858 unlensed SCAT 500 μm sources in Lockman which are associated with SWIRE galaxies (or QSOs). The 368 unassociated SCAT sources have been shown, arbitrarily, distributed uniformly between redshift 1.5 and 5. Fig. 24 (right) shows the redshift distribution for the 109 candidate lenses (in blue) and for the candidate lensed galaxies (in red) based on an Arp 220 fit to the submillimetre data.

Fig. 25 (left) shows the distribution of infrared luminosity (1–1000 μm), $L_{\rm ir}$, with redshift for the 858 unlensed SCAT 500 μm sources in Lockman which are associated with SWIRE galaxies (or QSOs), colour-coded with the dominant contribution to the luminosity. The absence of sources to the lower right reflects the selection effects at 24, 350, and 500 μm, which are different for each template type. 598 galaxies (70 per cent) are ultraluminous ($L_{\rm ir} > 10^{12}\,{\rm L}_{\odot}$) and 225 (26 per cent) are hyperluminous ($L_{\rm ir} > 10^{13}\,{\rm L}_{\odot}$). 295 sources (34 per cent) are dominated by cirrus components, mostly cool ($\psi = 1$) or cold ($\psi = 0.1$) dust (only 46 of these were fitted by the warmer ($\psi = 5$) dust characteristic of our Galaxy). Thus, 500 μm selection favours galaxies with cooler interstellar dust than our own Galaxy.

By contrast, for 60303 *IRAS* Faint Source Catalog (FSC) galaxies selected at 60 μm (Wang & Rowan-Robinson 2009, Wang & Rowan-Robinson 2014), 8 per cent are ultraluminous, and 0.7 per cent are hyperluminous. Only four *IRAS* FSC galaxies are definitely known to be lensed. 42 per cent are dominated by cirrus components, but only 6 per cent of these cirrus galaxies require cooler dust. Just 4 per cent of *IRAS* galaxies have $z > 0.3$, compared with 88 per cent of unlensed 500 μm galaxies. Of course the surface density of *IRAS* FSC sources, 2.0 deg^{-2}, is very different from that of the Lockman-HerMES survey at 500 μm, 180 deg^{-2}. But over 80 per cent of *IRAS* FSC galaxies have $z < 0.1$, and the surface density of Lockman-HerMES 500 μm galaxies with $z < 0.1$ is only 3.9 deg^{-2}, so the surveys are quite well-matched in terms of the surface-density of nearby galaxies. It is clear that a wavelength of 500 μm provides a dramatically different picture of the infrared

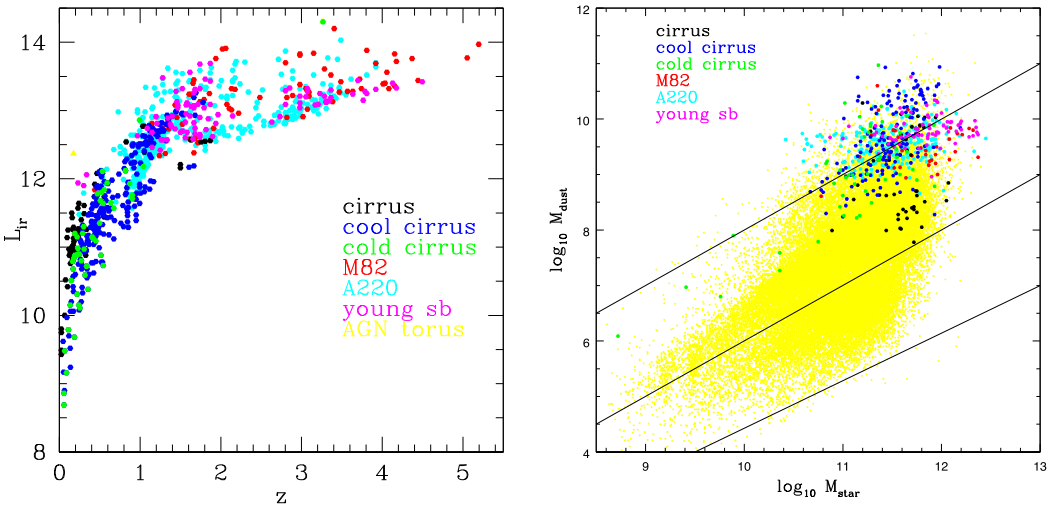

Figure 25. Left hand: the distribution of infrared luminosity, L_{ir}, with redshift for the 858 SCAT 500 μm sources in Lockman which are associated with unlensed SWIRE galaxies. Black: cirrus ($\psi = 5$); blue: cirrus ($\psi = 1$); green: cirrus ($\psi = 0.1$); red: M82 starburst; cyan: Arp 220 starburst; magenta: young starburst; yellow: AGN dust torus. Right hand: $\log_{10}M_{dust}$ versus $\log_{10}M_{star}$, in solar units, for HerMES-Lockman galaxies superposed on distribution for whole SWIRE catalogue (yellow points).

galaxy population, with its window on high redshifts, very high luminosities, and colder galaxies, to that seen by *IRAS* at 60 μm.

Having submillimetre fluxes not only gives us key diagnostic information on the nature of the infrared emission from galaxies, it also allows us to estimate the dust mass far more accurately. Fig. 25 (right) shows dust mass, calculated from our radiative transfer models as in Rowan-Robinson et al. (2010, 2013), versus stellar mass calculated from our stellar synthesis optical–NIR galaxy templates (Rowan-Robinson et al. 2008). The *Herschel* galaxies lie at the upper end of the dust-mass distribution seen for all SWIRE galaxies, shown as a yellow distribution. Much deeper submillimetre surveys would be needed to sample the full range of dust masses in galaxies.

Our results are not directly comparable with most other studies of the SEDs of SPIRE sources. Hwang et al. (2010), Symeonidis et al. (2013), and Magnelli et al. (2014) fit SEDs with a modified blackbody. Conclusions about correlation of 'dust temperature' with infrared luminosity or redshift correspond in our approach to variations in the proportions of different components. The modified blackbody approach gives no insight into whether the dust has high or low optical depth, or whether the galaxy is in a starburst or quiescent phase. Magdis et al. (2013) have studied a sample of 330 galaxies with $S(24) > 5$ mJy in the SWIRE areas for which *Spitzer*-IRS data are available. Just 2 per cent of our sample are this bright at 24 μm and there is no overlap with our sample. Their conclusions mainly concern PAH strength and AGN content.

We show the 500 μm differential source-counts for 858 unlensed Lockman-SCAT-SWIRE sources + the 368 unassociated SPIRE sources, and for the 109 candidate lensed galaxies (Fig. 26). The total number of potential lenses, 24 μm galaxies with redshift between 0.15 and 0.95 is 28 549, so the total area surveyed for lenses is found by multiplying this by the solid angle subtended by a typical Einstein ring. For $z_{lens} \sim 0.5$, $z_{image} \sim 3.0$, $M_{lens} = 4.10^{11}$ $M_{\odot}$ (allowing for the dark matter contribution), we estimate the radius of a typical Einstein ring as ∼1.4 arcsec. This yields a fraction of the 7.53 deg^2 surveyed for lenses as 1:520. This estimate is consistent with the lensing probability estimated from the CLASS survey by Browne et al. (2003) of 1:690 ± 190. From Wardlow et al. (2013), we estimate that a mean lensing magnification of 5 is appropriate for our $S(500) = 25$mJy selection. As a consistency check we have therefore shown the lensed galaxy counts corrected by this amount in flux-density, and by the factor 520 in number, i.e. we are demagnifying the observed counts of lensed objects and scaling by the lensed fraction to give a crude estimate of the unlensed counts for these objects. The resulting combined lensed and unlensed counts are plausible when compared with a compilation of observed counts and with source-count models (e.g. Rowan-Robinson 2009). However, they are also consistent with as many as 50 per cent of lens candidates with $S500 < 50$ mJy being chance associations.

Gonzalez-Nuevo et al. (2012) have used SED arguments (but without the benefit of the all-important 3.6–24 μm data) to define lens candidates down to $S500 \sim 60$ mJy in the H-ATLAS survey, at a surface density of ∼2 sources deg^{-2}. Our lens candidate sample is much deeper, at 25 mJy, and with a surface-density ∼14 deg^{-2}.

7 CONCLUSION

We have studied in detail a sample of 967 SPIRE sources with 5σ detections at 350 and 500 μm, and associations with SPIRE 24 μm galaxies, in the HerMES-Lockman survey area, fitting their mid- and far-infrared, and submillimetre, SEDs with a set of seven infrared templates. Details of a full data table for the sample are given at http://astro.ic.ac.uk/public/mrr/HermesLockmanreadme. For almost 300 galaxies, we have modelled their SEDs individually. We confirm the need for the new cool and cold cirrus templates, and also of the young starburst template, introduced by Rowan-Robinson et al. (2010). We also identify 109 lensing candidates via their anomalous SEDs and provide a set of colour–redshift constraints which allow lensing candidates to be identified from combined *Herschel* and *Spitzer* data. The lensing candidates and the galaxies requiring cold dust to understand their SEDs need to be confirmed with submillimetre interferometry, optical or NIR imaging, and submillimetre or optical spectroscopy.

The picture that emerges of the submillimetre galaxy population is complex, comprising ultraluminous and hyperluminous starbursts, lower luminosity galaxies dominated by interstellar dust emission, lensed galaxies and galaxies with surprisingly cold (10–13 K) dust. 11 per cent of 500 μm selected sources are lensing candidates. 70 per cent of the unlensed sources are ultraluminous

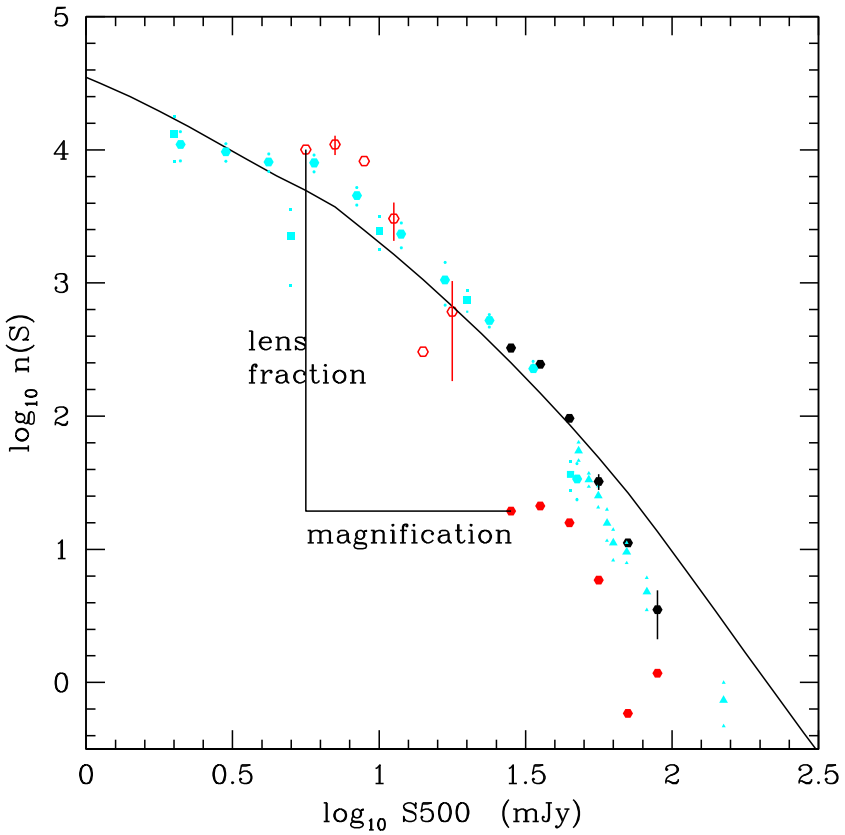

Figure 26. The 500 μm differential counts ($n(S) = \mathrm{d}N/\ln S$, deg^{-2}) for 858 unlensed Lockman-SCAT-SWIRE sources + the 368 unassociated sources (black filled circles) and lensed galaxies (red filled circles), The latter have also been shown corrected for an average lensing magnification of 5, and with the numbers multiplied by 520 to correct for the fraction of the Lockman area that is imaged by potential lensing galaxies (red open circles). A compilation of HerMES and ATLAS differential counts (Bethermin, private communication) is also shown (cyan symbols). A representative count model prediction (Rowan-Robinson 2009) is also shown (solid curve).

infrared galaxies and 26 per cent are hyperluminous. 34 per cent are dominated by optically thin interstellar dust ('cirrus') emission, but most of these are due to cooler dust than is characteristic of our Galaxy. At the highest infrared luminosities, we see SEDs dominated by M82, Arp 220 and young starburst types, in roughly equal proportions.

ACKNOWLEDGEMENTS

SPIRE has been developed by a consortium of institutes led by Cardiff Univ. (UK) and including Univ. Lethbridge (Canada); NAOC (China); CEA, LAM (France); IFSI, Univ. Padua (Italy); IAC (Spain); Stockholm Observatory (Sweden); Imperial College London, RAL, UCL-MSSL, UKATC, Univ. Sussex (UK); Caltech, JPL, NHSC, Univ. Colorado (USA). This development has been supported by national funding agencies: CSA (Canada); NAOC (China); CEA, CNES, CNRS (France); ASI (Italy); MCINN (Spain); SNSB (Sweden); STFC (UK); and NASA (USA). The Dark Cosmology Centre (JW) is funded by the Danish National Research Foundation.

The data presented in this paper are available through the *Herschel* Database in Marseille HeDaM.[3]

SJO acknowledges support from the Science and Technology Facilities Council (grant numbers ST/L000652/1) and from the European Commission Research Executive Agency REA (Grant Agreement Number 607254).

EI acknowledges funding from CONICYT/FONDECYT postdoctoral project no.: 3130504.

[3] hedam.oamp.fr/HerMES

REFERENCES

Ade P. A. R. et al., 2011, A&A, 536, 16
Browne I. W. A. et al., 2003, MNRAS, 341, 13
Dale D. A., Helou G., Contursi A., Silbermann N. A., Kolhatkar S., 2001, ApJ, 549, 215
Dopita M. A. et al., 2005, ApJ, 619, 755
Dowell C. D. et al., 2014, ApJ, 780, 75
Draine B. T., Li A., 2006, ApJ, 657, 810
Dullemond C. P., van Bemmel I. M., 2005, A&A, 436, 47
Efstathiou A., Rowan-Robinson M., 1995, MNRAS, 273, 649
Efstathiou A., Rowan-Robinson M., 2003, MNRAS, 343, 322
Efstathiou A., Rowan-Robinson M., Siebenmorgen R., 2000, MNRAS, 313, 734
Efstathiou A., Siebenmorgen R., 2009, A&A, 502, 541
Farrah D. et al., 2008, ApJ, 677, 957
Franceschini A. et al., 2005, AJ, 129, 2074
Fritz J., Franceschini A., Hatziminaoglou E., 2006, MNRAS, 366, 767
Gonzalez-Nuevo J. et al., 2012, ApJ, 749, 65
Granato G. L., Danese L., 1994, MNRAS, 268, 235
Griffin M. J. et al., 2010, A&A, 518, L3
Griffin M. J. et al., 2013, MNRAS, 434, 992
Hernan-Caballero A. et al., 2009, MNRAS, 395, 1695
Hönig S. F., Beckert T., Ohnaka K., Weigelt G., 2006, A&A, 452, 459

Hwang H. S. et al., 2010, MNRAS, 409, 75
Lonsdale C. et al., 2003, PASP, 115, 897
Magdis G. E. et al., 2012, ApJ, 760, 6
Magdis G. E. et al., 2013, A&A, 558, 136
Magnelli B. et al., 2014, A&A, 561, 86
Negrello M., Perrotta F., González-Nuevo J., Silva L., de Zotti G., Granato G. L., Baccigalupi C., Danese L., 2007, MNRAS, 377, 1557
Negrello M. et al., 2010, Science, 330, 800
Nenkova M., Ivezic Z., Elitzur M., 2002, ApJ, 570, L9
Nenkova M., Sirocky M. M., Ivezić Ž., Elitzur M., 2008, ApJ, 685, 147
Nguyen H. T. et al., 2010, A&A, 518, L5
Oliver S. J. et al., 2012, MNRAS, 424, 1614
Piazzo L., Ikhenaode D., Natoli P., Pestalozzi M., Piacentini F., Traficante A., 2012, IEEE Trans. Image Process., 21, 3687
Pier G. L., Krolik J., 1992, ApJ, 401, 99
Pilbratt G. et al., 2010, A&A, 518, L1
Piovan L., Tantalo R., Chiosi C., 2006, MNRAS, 366, 923
Poglitsch A. et al., 2010, A&A, 518, L2
Polletta M. et al., 2007, ApJ, 663, 81
Roseboom I. et al., 2010, MNRAS, 409, 48
Rowan-Robinson M., 1992, MNRAS, 258, 787
Rowan-Robinson M., 1995, MNRAS, 272, 737
Rowan-Robinson M., 2001, ApJ, 549, 745
Rowan-Robinson M., 2009, MNRAS, 394, 117
Rowan-Robinson M., Crawford J., 1989, MNRAS, 238, 523
Rowan-Robinson M., Efstathiou A., 1993, MNRAS, 263, 675
Rowan-Robinson M., Efstathiou A., 2009, MNRAS, 399, 615
Rowan-Robinson M. et al., 2004, MNRAS, 351, 1290
Rowan-Robinson M. et al., 2005, AJ, 129, 1183
Rowan-Robinson M., 2008, in Chary R.-R., Teplitz H. I., Sheth K., eds, ASP Conf. Ser. Vol. 381, Infrared Diagnostics of Galaxy Evolution. Astron. Soc. Pac., San Francisco, p. 216
Rowan-Robinson M. et al., 2008, MNRAS, 386, 697
Rowan-Robinson M. et al., 2010, MNRAS, 409, 2
Rowan-Robinson M., Gonzalez-Solares E., Vaccari M., Marchetti L., 2013, MNRAS, 428, 1958
Schartmann M., Meisenheimer K., Camenzind M., Wolf S., Tristram K. R. W., Henning T., 2008, A&A, 482, 67
Siebenmorgen R., Krugel E., 2007, A&A, 461, 445
Silva L., Granato G. L., Bressan A., Danese L., 1998, ApJ, 509, 103
Spoon H., Marshall J. A., Houck J. R., Elitzur M., Hao L., Armus L., Brandl B. R., Charmandaris V., 2007, ApJ, 654, L49
Symeonidis M., Page M. J., Seymour N., Dwelly T., Coppin K., McHardy I., Rieke G. H., Huynh M., 2009, MNRAS, 397, 1728
Symeonidis M. et al., 2013, MNRAS, 431, 2317
Takagi T., Arimoto N., Hanami H., 2003, MNRAS, 340, 813
Wang L., Rowan-Robinson M., 2009, MNRAS, 398, 109
Wang L., Rowan-Robinson M., Norberg P., Heinis S., Han J., 2014, MNRAS, 442, 2739
Wang L. et al., 2014, MNRAS, 444, 2879
Wardlow J. L. et al., 2013, ApJ, 762, 59

SUPPORTING INFORMATION

Additional Supporting Information may be found in the online version of this article:

(http://mnras.oxfordjournals.org/lookup/suppl/doi:10.1093/mnras/stu1959/-/DC1).

Please note: Oxford University Press are not responsible for the content or functionality of any supporting materials supplied by the authors. Any queries (other than missing material) should be directed to the corresponding author for the article.

This paper has been typeset from a TEX/LATEX file prepared by the author.